Confined Immersion Cooling in Microscale Gaps

Albraa A. Alsaati, Justin A. Weibel, and Amy M. Marconnet

School of Mechanical Engineering
Purdue University
P.O. Box 12345
West Lafayette, IN, USA, 47907
Email: marconnet@purdue.edu

ABSTRACT

Thermal management is one of the major operational concerns for data centers and accounts for a significant fraction of total power consumption. Passive immersion cooling solutions have been explored owing to their potential for offering low overall thermal resistance in very dense rack configurations where there is no room for conventional heat sinks between printed circuit boards. Further, in practice, regions of high heat flux are localized to where processing units are positioned. Non-uniform heating, as well as local hot spots, could affect thermal performance as a result of the need for rewetting of the surface with liquid during boiling. This work explores immersion cooling in submillimeter confined liquid filled gaps with localized heat sources. Specifically, this work investigates the thermofluidic characteristics of highly confined boiling surfaces. A camera is used to visualize the two-phase flow regimes and instabilities that occur prior to critical heat flux (CHF) limits. Two distinct boiling regimes are observed (namely, intermittent boiling and partial dryout). Both the heated fraction of the area within the confined region and the gap spacing affect the CHF values and thermal performance prior to CHF. The optimum thermal performance, in terms of the surface superheat, is experimentally observed for a confinement corresponding to a Bond number of 0.2. However, at this optimum condition based on surface superheat, the CHF is significantly reduced to 27% of the unconfined CHF limit. Significant additional reductions in the CHF are also experimentally observed when the adiabatic confinement surface is extended beyond the heater edge. This additional fundamental understanding of the impact of spatial confinement on the thermal performance of immersion cooling has broad implications for two-phase thermal management solutions.

KEY WORDS: confined boiling, Bond number, electronics cooling, data centers, critical heat flux (CHF).

NOMENCLATURE

A	area
Bo	Bond number, S/L (-)
D	diameter (m)
g	gravitational acceleration (m/s^2)
h_{vl}	latent heat of vaporization (J/kg)
L	capillary length (m)
$q"$	heat flux (W/m^2)
$q"_{CHF}$	critical heat flux (W/m^2)
S	confinement gap size (m)
T	temperature (°C)
ρ	mass density (kg/m^3)
σ	surface tension (N/m)

Subscripts

b	boiling surface
c	confinement window
l	liquid
v	vapor
sat	saturation condition

INTRODUCTION

In the modern digital era, data centers are an indispensable resource for almost any organization. The global market for cloud and data center networks was valued at $17 billion in 2017 and growing annually at 15% [1]. US-based data centers alone are projected to consume 73 billion kWh in 2020 (an equivalent to 1.8% of total US electricity consumption) [2, 3]. Cooling is estimated to account for nearly a quarter of the total power consumption of data centers [4]. In addition to energy cost, inadequate data center cooling solutions limit computing performance and reliability. Since the early 1990's, thermal management of complementary metal–oxide–semiconductor (CMOS) based processing electronics have increasingly become the bottleneck for increasing the processing power [5]. New products and improved controls on air cooling of data centers have expanded the performance limits while providing energy savings. However, room-based approaches that condition the bulk air do not exploit the performance advantages of liquid cooling solutions applied nearer the hot surfaces of high-power electronics [6]. Additionally, rack-based liquid-cooling solutions provide the flexibility for segmenting the cooling load within the data center [2].

Currently, two-phase liquid cooling is an active research area both in academia and industry due to the improved maximum heat flux dissipation limits. In fact, researchers have demonstrated intra-chip flow boiling solutions using dielectric coolants for hotspot heat fluxes up to 2500 W/cm^2 [7, 8, 9, 10, 11, 12]. However, a radical change to electronics packaging approaches would be required to achieve this level of thermal performance. Any active two-phase cooling approach would further require pumps, hoses, manifolds, couplings, and other components. Passive immersion cooling has the potential to simplify two-phase cooling design by eliminating much of this additional hardware. Immersion cooling solutions become viable and attractive for cooling computing systems with very high rack packing density [13].

Passive liquid immersion cooling solutions require an understanding of boiling phenomena in highly confined spaces [14, 15]. In comparison to the extensive research on unconfined pool boiling, the existing literature focusing on confined boiling

A. Alsaati, J. A. Weibel, and A. Marconnet, "Confined Immersion Cooling in Microscale Gaps", IEEE- The Intersociety Conference on Thermal and Thermomechanical Phenomena in Electronic Systems (ITherm) Proceedings, 2020

is sparse. Katto et al. [16] performed one of the earliest confined boiling studies and showed that confinement improves the heat transfer coefficient while reducing CHF. Later studies demonstrated that confined boiling has less sensitivity to the surface orientation [17] and roughness [18] compared to unconfined conditions; however, nanostructured surfaces significantly improve the heat transfer coefficient of confined boiling [19]. Furthermore, the area of confined boiling has been found to be inversely correlated to CHF for uniform heating [20]. On the other hand, confinement has been shown to reduce heat transfer coefficient for subcooled conditions [21]. Further mechanistic understanding of the confined boiling regimes leading to these trends, as well as the effect of non-uniform heat fluxes, are crucial for implementing confined immersion cooling.

The aim of this study is to identify and characterize boiling regimes for confined boiling and to understand the effect of heat source size with respect to the confined zone. We measure boiling curves for various confinement levels (i.e., the distance between the heated surface and a confining plate) and visually observe the boiling regimes to understand the heat transfer enhancement mechanisms. The study further aims to identify the confinement geometry that results in a minimum surface superheat.

EXPERIMENTAL SETUP

Figure 1 shows the experimental facility for the confined immersion cooling experiments. The facility enables measurement of the boiling curve (heat flux and surface superheat) while controlling the confinement gap size, S, and the confinement diameter, D_c, and fixing the boiling diameter, D_b. To elucidate the confined boiling characteristics, the facility is equipped with a camera for visualizing the dynamic two-phase interfaces within the confinement gap.

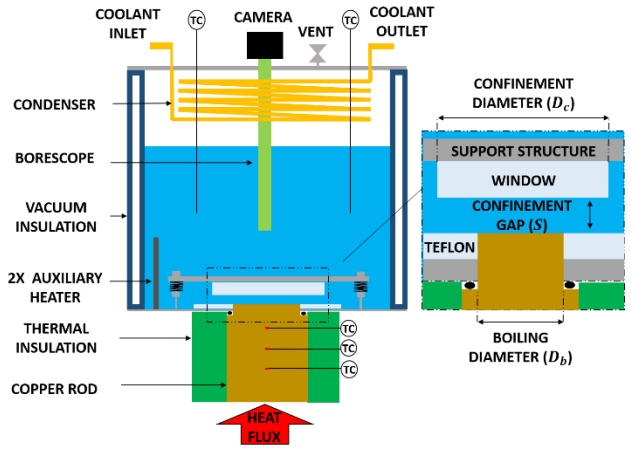

Figure 1: Schematic illustration of the confined boiling experimental facility. Cartridge heaters (not shown) provide heat to the copper rod from below. The heat flux and the boiling surface temperature are measured from thermocouples embedded in the copper rod. Thermal insulation surrounding the rod minimizes the radial temperature gradient and heat losses. An adjustable glass window confines boiling to within a controlled gap above the boiling surface. A camera captures the two-phase interfaces in the confinement gap as viewed through a rigid borescope. The pool of water is maintained at the saturation temperature using two auxiliary cartridge heaters with temperature control based on the thermocouples within the pool.

The 25.4 mm-diameter boiling surface is oriented horizontally at the bottom of a double-wall vacuum-insulated quartz glass cylinder chamber with an approximate volume of 500 mL and inner diameter of 75 mm. The chamber is filled with deionized water (0.37 µS/cm) consistently to a level of 10 cm above boiling surface.

A 1000 W cartridge heater (Watlow Firerod 1039; 1.27 cm diameter, 7.62 cm length) supplies heat to the boiling surface through the 31.75 mm-diameter and 107.95 mm-height copper rod. Three T-type thermocouples (Omega; ±0.3 K) embedded at the centerline of the copper reference rod, spaced 6.35 mm apart along rod axis, measure the temperature gradient, which is linearly correlated to the heat flux at steady state according to Fourier's law assuming one-dimensional heat flow. The radial non-uniformity in temperature at the thermocouple locations is numerically estimated to be more than an order of magnitude less than the thermocouple uncertainty. Using the measured temperature gradient to calculate the heat flux accounts for heat losses through the insulation. A DAQ (Labjack U6pro) logs the temperature measurements through Labview at a 1 Hz sampling rate. The surface temperature is linearly extrapolated from the reference rod temperature measurements using a (numerically estimated) thermal resistance of the stepped cylinder of copper beyond the topmost thermocouple which is placed 12.7 mm below the boiling surface. To limit radial conduction within the reference rod, a 1.8 cm-thick microporous insulation (MICROSIL) surrounds the rod. The reference rod is sealed to the boiling chamber with a Viton O-ring at the step in the rod diameter.

In each experiment, a 6.35 mm-thick circular glass window is suspended above the boiling surface with an adjustable gap size, S, to provide confinement of the fluid above the boiling surface. The diameter of the window varies from the same diameter as the copper rod (25.4 mm) to 50.8 mm in diameter; this is used to control and study the effect of the relative area of the boiling surface to the confined region. The step of the copper rod protrudes 5.5 mm above the chamber base. A Teflon ring flush with the top of the boiling surface maintains a constant confinement gap throughout an extended region beyond the confinement window, providing an adiabatic boundary around the periphery of the boiling surface (see Figure 1 inset). Both the inner and outer diameter of the Teflon ring are sealed with a high temperature sealant (Permatex 81160). Three spring-loaded set screws adjust and level the confinement gap with a resolution of 2.2 µm/degree. The confinement gap size is adjusted using reference stainless steel shims. The glass window and glass boiling chamber permit optical access to the two-phase test section. The two-phase interfaces are visualized at 480 frames per second through a rigid borescope (Hawkeye Pro Hardy) where the objective lens is submerged in the liquid pool.

A chiller (PolyScience AD07R-40-A11B) circulates 90°C cooling water through a copper coil heat exchanger enclosed inside the top of the boiling chamber to condense vapor back to the liquid pool. The facility body is electrically grounded to prevent charge accumulation and reduce measurement noise. Two submerged auxiliary cartridge heaters (Omega HDC19110; 0.32 cm diameter, 8.89 cm length) along with two T-type thermocouples (Omega; ±0.3 K) maintain the liquid

pool at saturation conditions under atmospheric pressure. The chamber is maintained at atmospheric pressure through an open vent as shown in Figure 1.

Prior to collecting boiling data, the working fluid is boiled vigorously using the auxiliary heaters to purge all non-condensable gasses trapped in the confined gap and dissolved in the liquid. The degassing process is maintained for a minimum of 2 hr producing a saturated water vapor condition. The working fluid is considered degassed when the boiling temperature reaches within 0.3 °C of the pure liquid saturation temperature. Once the fluid is degassed, the auxiliary heaters are controlled to maintain saturation condition in the chamber.

The boiling curve data points correspond to a fixed input heat flux where temperature measurements are stable (*i.e.*, temperature measurements change less than 0.1°C/min for a duration of 10 min). After reaching steady state for every data point on the boiling curve, the camera records the two-phase interfaces during boiling. This steady state measurement is repeated with increasing input powers to obtain the entire boiling curve for each case presented in the results. At each increment, the main heater is turned off momentarily (~20 s) and then powered to the next heat flux level. During testing, the heat flux is increased until CHF is reached, as indicated by a very steep temperature rise and confirmed via visualization of film boiling. Finer power increments are used around the incipience of boiling and CHF to improve the resolution of identifying these transitions.

RESULTS AND DISCUSSION

Unconfined Pool Boiling Benchmark Testing

Prior to conducting the confined boiling measurements, the experiments are performed for an unconfined pool boiling condition without the glass window in place. Four repeated boiling curves plotting the applied heat flux (q'') as a function of the surface superheat (T_b - T_{sat}) are obtained to demonstrate repeatability (see Figure 2). The highest heat flux value in each measurement run is taken as the CHF, as the next increment in heat flux results in complete coverage of the boiling surface with a vapor film. The variation of measured CHF values for this unconfined boiling configuration is found to be within ±6.6% of average. The average measured CHF value is also compared to the theoretical prediction proposed by Lienhard and Dhir [22]:

$$q''_{CHF} = \frac{\pi}{24}\,\rho_v h_{lv}\left[\frac{\sigma\,(\rho_l-\rho_v)g}{\rho_v^2}\right]^{\frac{1}{4}}. \qquad (1)$$

The average measured CHF value (96.8 W/cm^2) is within 12.5% of theoretical prediction (110.7 W/cm^2). These unconfined boiling curves serve as a baseline for comparison to the confined boiling cases.

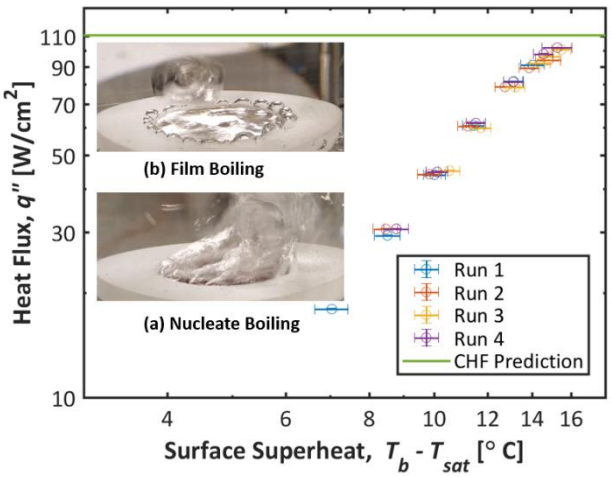

Figure 2: Experimental facility repeatability tests for the unconfined pool boiling curve. The highest heat flux value in each run represents the critical heat flux (CHF) compared to the theoretical prediction (green line). The inset images show the transition from (a) nucleate boiling to (b) film boiling following an increment to a heat flux higher than CHF.

Confined Boiling Characterization

Confined boiling curves are measured for four confinement gaps ranging from 128 µm to 762 µm. For this set of tests, the confinement window has the same area as the boiling surface (A_b/A_c = 1) and is aligned directly above. For the presentation of confined boiling data, the gap size, S, is normalized by the capillary length, L, of the fluid to yield the nondimensional Bond number,

$$Bo = \frac{S}{L} = \frac{S}{\sqrt{\frac{\sigma}{g(\rho_l-\rho_v)}}}\ . \qquad (2)$$

A Bond number much larger than unity indicates that the size vapor bubbles that depart from the boiling surface are much smaller than the gap size (or in the case of unconfined boiling, freely depart from the surface). However, for Bond numbers on the order of unity or less, these length scales are similar and the confinement wall will interface with the vapor bubbles generated at the boiling surface [16]. In this study, a range of Bond number from 0.05 (corresponding to S = 128 µm) to 0.30 (S = 762 µm) is investigated.

Boiling curves are shown in Figure 3 for multiple different Bond numbers (i.e., degrees of confinement). The unconfined boiling curve is plotted as a dashed line for reference. As a general trend, the surface superheat is lower for the confined cases compared to the unconfined boiling case at similar heat fluxes. However, the critical heat flux is significantly reduced when boiling is confined. From interpretation of the boiling curve data alongside the optical visualizations, two distinct boiling regimes are identified for confined boiling beyond natural convection regime: intermittent boiling and partial dryout.

Like unconfined boiling, the natural convection regime (gray shaded region of Figure 3) is characterized by a lack of boiling within the gap at elevated surface superheats. At low heat flux values (approximately less than 10% of confined boiling CHF), heat is dissipated through conduction and single-phase natural convection. At higher heat flux values, the surface superheat becomes large enough to initiate nucleation within the confined space.

Upon vapor nucleation, there is a transition to the intermittent boiling regime (green shaded region of Figure 3). This boiling regime exhibits a time-periodic oscillatory

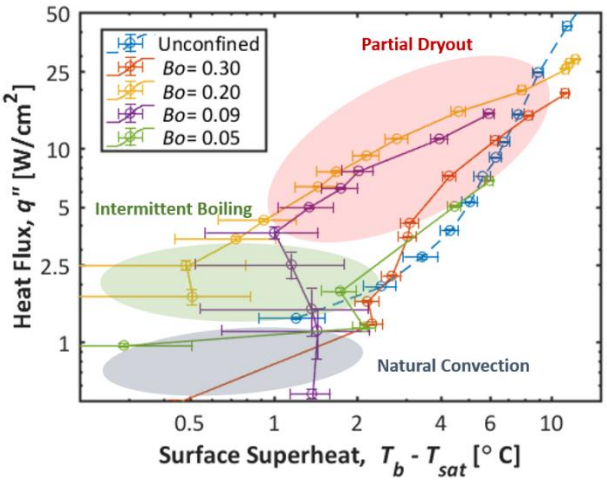

Figure 3: Boiling curve for different nondimensional confinement gaps sizes ($Bo = S/L$) are shown as solid lines. Natural convection (gray shaded region) is observed at low heat fluxes where no nucleation sites are activated. During intermittent boiling (shaded in green), vapor is generated slowly enough that the entire boiling surface is able to rewet following periodic vapor departure from the gap. Finally, as the vapor generation frequency increases, the boiling transition to partial dryout regime (shaded in red) where regions of the boiling surface remain continually covered with vapor. The unconfined boiling curve is shown in blue as a dashed line for reference (regimes do not apply).

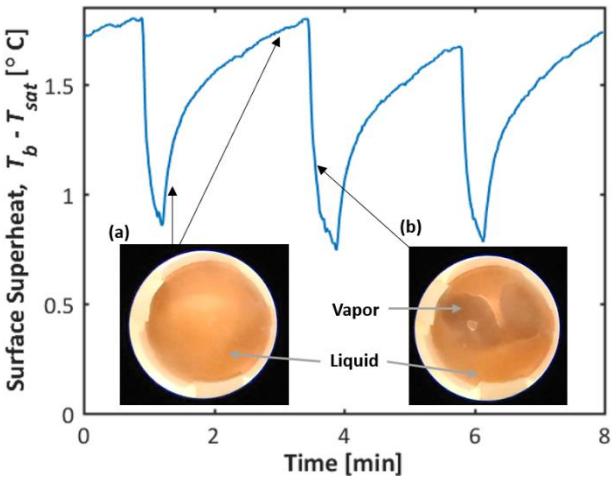

Figure 4: Surface temperature oscillations in the intermittent boiling regime (Bo = 0.09, q''=1.5 W/cm^2). In the portions of the data where the surface temperature rises with time, the confined liquid is heated without phase change (inset (a)) until the minimum required superheat for nucleation is reached. Inset (b) illustrates the nucleation of vapor bubbles that escape from confinement region and are replaced by a sudden inrush of saturated liquid from surrounding pool that quenches the boiling surface.

behavior at steady state, as observed both through the transient boiling surface temperature measurements and the visualizations (see Figure 4). During these oscillations, the temperature of the liquid within the confined cavity rises until it reaches the minimum required superheat to achieve nucleation. Then, vapor bubbles nucleate and expand radially outward until reaching the outer periphery of the confinement window, where surface tension and buoyancy forces facilitate extraction of vapor from the confined region into the liquid pool. Consequently, liquid from the surrounding pool flows radially inward to fill the volume displaced by the departed vapor bubble. This capillary-assisted radial inward flow of liquid at the saturation temperature has a quenching effect on the boiling surface, lowering its temperature below the required nucleation temperature. This process repeats in a cyclic manner. As the heat flux increases, the frequency of this oscillatory behavior increases. The boiling curve in this complete rewetting regime exhibits a negative slope (*i.e.*, reducing time-averaged superheat with increasing heat flux) as a result of the higher quenching frequencies at higher heat fluxes.

As the frequency of vapor generation further increases at higher heat fluxes, the capillary forces are insufficient to overcome the viscous resistance and maintain complete rewetting of the surface with liquid as vapor escapes the confinement gap. Consequently, some regions of the boiling surface remain covered with vapor and the boiling behavior transitions into the partial dryout regime (red shaded region of Figure 3). The dry area is most often observed at the center of the boiling surface – that is, the locations with the largest distance from the confinement window edge. As observed from the visualizations, the percentage of dry area to wetted area increases as heat flux values increases, resulting in higher average steady state temperatures as demonstrated in the confined boiling curves. Confinement has a severe deleterious effect on the critical heat flux, with a severity that depends on the confinement gap size. Nevertheless, of all confinement gaps tested, the maximum measured CHF is only 27% of the unconfined CHF.

Confined Boiling Heat Transfer Enhancement.

As demonstrated with the boiling curves (Figure 3), confined boiling typically maintains the surface at a lower temperature compared to unconfined boiling prior to CHF. The enhancement in confined heat transfer is attributed to two potential mechanisms illustrated in Figure 5. The high heat transfer rates associated with nucleate boiling is widely attributed to microlayer evaporation near the three-phase contact line [24, 25]. In confined boiling, the confinement window above the boiling surface restricts the vapor bubble growth normal to the boiling surface. Hence, the vapor bubble is forced to grow radially along the boiling surface from the point of nucleation. This elongates the thin liquid layer on the boiling surface underneath the bubble (also known as the microlayer); see Figure 5(a). As a result, confined vapor bubbles have larger microlayer areas compared to the unconfined case where bubbles can freely depart from the boiling surface.

The second enhancement mechanism is the nucleation-enhanced rewetting. Vapor nucleation first occurs on a portion of the confinement gap filled with liquid. Rapid volume expansion due to phase change at a nucleation site is observed

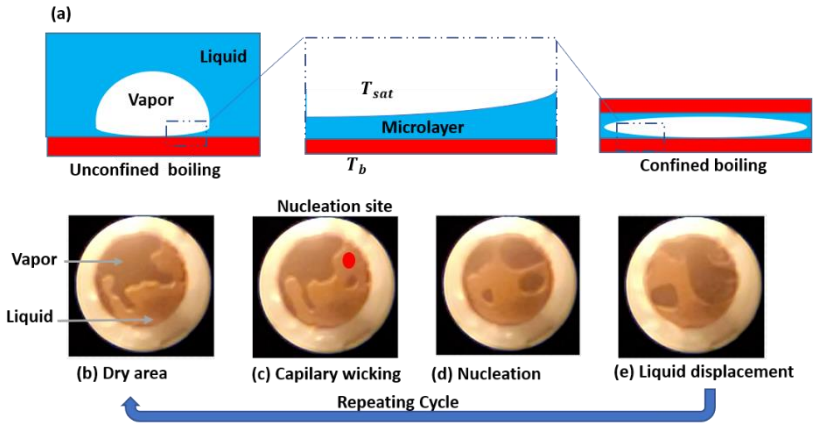

Figure 5: Confined boiling heat transfer enhancement mechanisms. (a) Confinement induces radial growth of vapor bubbles enlarging the microlayer coverage compared to unconfined boiling. (b-e) A time series of images that illustrate nucleation-enhanced rewetting where the volume expansion during phase change at nucleation site (red dot) displaces liquid from wet areas to dry areas.

to force liquid to rewet dry regions of the boiling surface, as shown in the time series of images in Figure 5(b-d). As a result, dry spots reside on the boiling surface for a shorter duration, lowering the average surface temperature.

Impact of Confinement Gap and Window Size

Both the fraction of the area within the confined region heated by the boiling surface (A_b/A_c) and gap spacing (S) affect the CHF values and thermal performance prior CHF.

In practice, regions of high heat flux generation on immersion-cooled electronic boards are localized where processing units are positioned. To understand how the relative size of localized heated regions affect the thermal performance of highly confined immersion cooling solutions, boiling curves are obtained for cases where the confinement window size is extended beyond the heater edge. This study investigates an extension range from A_b/A_c = 1 to A_b/A_c = 0.25. The results indicate that positioning heat sources further from the edge of the confinement region has detrimental consequences on the performance under confined boiling conditions. Generally, the boiling curves for the extended confinement window size (not shown) illustrate the same boiling regimes previously discussed. However, at any given degree of confinement, CHF is observed to be significantly lowered when the confinement window is extended, as shown in Figure 6.

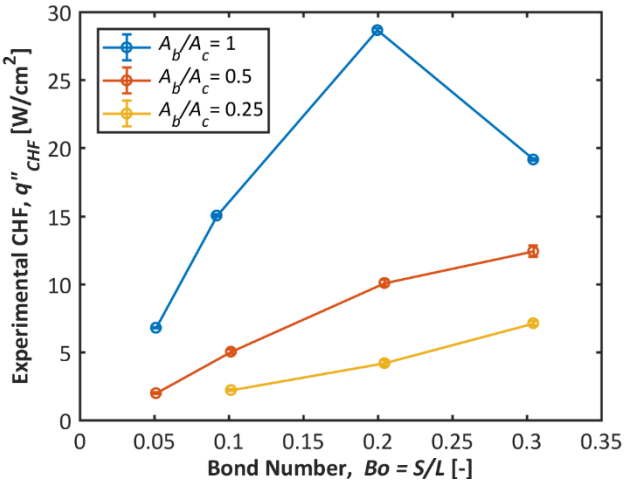

Figure 6: Influence of confinement gap size on the CHF for differing fractions of the area within the confined region heated by the boiling surface.

The thermal performance of confined boiling is highly sensitive to confinement. Two physical phenomena are correlated to the degree of confinement: the capillary pressure generated in the gap that assists rewetting and the counteracting viscous resistance. To illustrate the impact of confinement on the boiling surface temperature, Figure 7 illustrates the interpolated surface superheats linearly interpolated from the boiling curves for multiple constant heat fluxes as a function of Bond number for (a) A_b/A_c = 1 and (b) A_b/A_c = 0.25. Consistently, there is a local minimum in surface superheat for the Bo = 0.2 indicating a tradeoff in the available capillary pressure and viscous resistance, which scale differently with the gap size S. At the minimum superheat, the confined fluid demonstrates the maximum ability for rewetting. Similar trends with Bond number are observed for the case where the confinement window extends beyond the boiling surface. These preliminary experimental results indicate that the optimum confinement gap is not sensitive to the heat flux or extension of the confinement area.

CONCLUSION

Boiling has been experimentally investigated under extremely confined gaps from 128 µm to 762 µm. Two distinct boiling regimes are identified. Similar to unconfined boiling, at low heat fluxes, heat is dissipated by conduction and natural convection. Once the boiling surface temperature reaches a minimum required superheat for nucleation, the boiling transitions into the intermittent boiling regime. This regime exhibits a time-periodic oscillatory behavior. Following vapor bubble departure from the confinement region, rewetting liquid from the surrounding pool lowers the surface superheat and

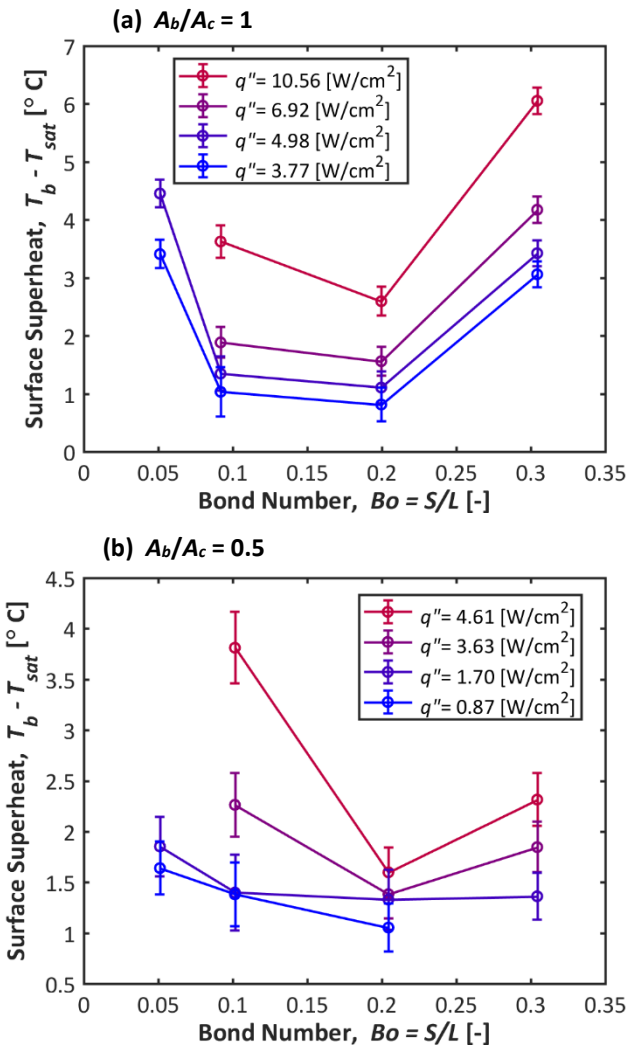

Figure 7: Influence of confinement gap size on the boiling surface superheat for differing heat fluxes. Cases are shown where (a) the boiling surface and confinement window are the same diameter and (b) where the boiling surface area is 1/2 of the confinement window area. A local minimum is observed near Bo = 0.2.

boiling ceases momentarily until the surface heats back up to the nucleation temperature. In this regime, higher heat flux values corresponded to high vapor generation frequencies, higher surface quenching frequencies, and lower time-averaged surface temperatures. Finally, in the partial dryout regime at higher heat fluxes, portions of the surface remain continually dried out, where the capillary forces are insufficient to overcome the viscous resistances necessary to completely rewet the surface as vapor is extracted from the gap at a high velocity.

Compared to unconfined pool boiling, the average confined boiling surface temperatures are lower at similar heat flux values. Nucleation-enhanced rewetting and a larger microlayer area are proposed to be the mechanisms for the enhanced thermal performance in confined boiling and merit further investigation. The optimum thermal performance is experimentally observed for a confinement gap size corresponding to a Bond number of 0.2. Despite a promising surface temperature reduction, the CHF for this optimum confinement gap size is only 27% of the unconfined CHF. Even more severe reductions in CHF are observed when the confinement region is extended to an area larger than the heater. Further investigation is recommended to improve the surface rewetting and increase CHF while preserving the heat transfer enhancement.

This improved fundamental understanding of geometrically confined boiling is important for the design of high-rack-density immersion cooling thermal solutions for data centers and other compact two-phase thermal management solutions.

Acknowledgments

This work was supported by Semiconductor Research Corporation (SRC), as a part of the Global Research Collaboration (GRC) Program on Packaging (PKG; Science Director, Dr. John Oakley) in the Center for Heterogeneous Integration Research on Packaging (CHIRP). A.A. acknowledges the support of a Saudi Arabia Cultural Mission (SACM) fellowship, sponsored by the Saudi Arabian Ministry of Education. Some components of the pool boiling fixture were adapted from a system originally developed by Prof. Timothy Fisher and colleagues as reported in [26].

References

[1] M. Sullivan, "Cloud and Data Center Network Technologies: Global Market Through 2022," BCC Research LLC, IFT103A, 2018.

[2] R. Rake, "North America Data Center Cooling Market by Component, Type of Cooling, Type of Data Center, Industry Vertical: Opportunity Analysis and Industry Forecast, 2018 - 2025," Allied Market Reserach, 2019.

[3] A. Shehabi, S. J. Smith, D. A. Sarto, R. E. Brown, M. Herrlin, J. G. Koomey, E. R. Masanet, N. Horner, I. L. Azevedo and W. Lintner, "United States Data Center Energy Usage Report," Lawrence Berkeley National Laboratory, Berkeley, California, 2016.

[4] L. A. Barroso, U. Hölzle, J. Clidaras and Parthasarathy, The Datacenter as a Computer: An Introduction to the Design of Warehouse-Scale Machines, third edition, Morgan & Claypool, 2018.

[5] S. V. Garimella, T. Persoons, J. A. Weibel and V. Gektin, "Electronics Thermal Management in Information and Communications Technologies: Challenges and Future Directions," IEEE Transactions on Components, Packaging and Manufacturing Technology, vol. 7, no. 8, pp. 1191-1205, 2107.

[6] H. C. Coles and S. E. Greenberg, "Direct Liquid Cooling for Electronic Equipment," Lawrence Berkeley National Laboratory, Berkeley, CA, 2014.

[7] D. H. Altman, A. Gupta and M. Tyhach, "Development of a Diamond Microfluidics-based Intra-chip Cooling Technology for GAN," in Proceedings of the ASME

International Technical Conference and Exhibition on Packaging and Integration of Electronic and Photonic Microsystems, San Francisco, California, USA, 2015.

[8] K. P. Drummond, D. Back, M. D. Sinanis, D. B. Janes, D. Peroulis, J. A. Weibel and S. V. Garimella, "Characterization of Hierarchical Manifold Microchannel Heat Sink Arrays Under Simultaneous Background and Hotspot Heating Conditions," International Journal of Heat and Mass Transfer, vol. 126, pp. 1289-1301, 2018.

[9] T. J. Chainer, M. D. Schultz, P. R. Parida and M. A. Gaynes, "Improving Data Center Energy Efficiency With Advanced Thermal Management," IEEE Transactions on Components, Packaging and Manufacturing Technology, vol. 7, no. 8, 2017.

[10] D. F. Hanks, Z. Lu, J. Sircar, T. R. Salamon, D. S. Antao, K. R. Bagnall, B. Barabadi and E. N. Wang, "Nanoporous Membrane Device For Ultra High Heat Flux Thermal Management," Microsyst Nanoeng, vol. 4, no. 1, 2018.

[11] P. Asrar, X. Zhang, C. E. Green, M. Bakir and Y. K. Joshi, "Flow Boiling of R245fa in a Microgap with Staggered Circular Cylindrical Pin Fins," International Journal of Heat and Mass Transfer, vol. 121, pp. 329-342, 2018.

[12] D. G. Bae, R. K. Mandel, S. V. Dessiatoun, S. Rajgopal, S. P. Roberts, M. Mehregany and M. M. Ohadi, "Embedded Two-phase Cooling of High Heat Flux Electronics on Silicon Carbide (SiC) Using Thin-film Evaporation and an Enhanced Delivery System (FEEDS) Manifold-microchannel Cooler," in 16th IEEE Intersociety Conference on Thermal and Thermomechanical Phenomena in Electronic Systems (ITherm), Orlando, FL, USA, 2017.

[13] G. R. Wagner, J. R. Schaadt, J. Dixon, G. Chan, W. Maltz, K. Mostafavi and D. Copeland, "Test Results From the Comparison of Three Liquid Cooling Methods for High-power Processors," in Proc. 15th IEEE Thermal and Thermomechanical Phenomena in Electronic Systems (ITherm), Las Vegas, NV, USA, 2016.

[14] H. Coles and M. Herrlin, "Immersion Cooling of Electronics in DoD Installation," Lawrence Berkeley National Laboratory, Berkeley, CA, 2017.

[15] P. E. Tuma, "The Merits of Open Bath Immersion Cooling of Datacom Equipment," in 26th Annual IEEE Semiconductor Thermal Measurement and Management Symposium (SEMI-THERM), Santa Clara, CA, USA, 2010.

[16] Y. Katto, S. Yokoya and K. Teraoka, "Nucleate and Transition Boiling in a Narrow Space Between Two Horizontal, Parallel Disk Surfaces," Bull. JSME, vol. 20, no. 143, pp. 638-643, 1977.

[17] E. Cardoso, O. Kannengieser, B. Stutz and J. Passos, "FC72 and FC87 Nucleate Boiling Inside a Narrow Horizontal Space," Experimental Thermal and Fluid Science, vol. 35, p. 1038–1045, 2011.

[18] M. Kapitz, L. Schmiedinghoff, S. J. Lüling and S. a. d. Wiesche, "Impact of Surface Parameters on Confined Boiling Heat Transfer in a Hele-Shaw Cell," Heart and Mass Transfer, vol. 55, pp. 2533-2544, 2019.

[19] R. Souzaa, E. Cardosob and J. Passos, "Confined and Unconfined Nucleate Boiling of HFE7100 in the Presence of Nanostructured Surfaces," Experimental Thermal and Fluid Science, vol. 91, pp. 312-319, 2018.

[20] M. Kapitz, F. Reinker and S. a. d. Wiesche, "Viscous fingering and heat transfer during boiling in a Hele–Shaw cell," Experimental Thermal and Fluid Science, vol. 67, pp. 18-23, 2015.

[21] J. Passos, F. Hirata, L. Possamai, M. Balsamo and M. Misale, "Confined boiling of FC72 and FC87 on a downward facing heating copper disk," International Journal of Heat and Fluid Flow, vol. 25, pp. 313-319, 2004.

[22] J. H. Linehard and V. K. Dhir, "Extended Hydrodynamic Theory of The Peak and Minimum Pool Boiling Heat Fluxes," NASA CR-2270, Washington, DC, USA, 1973.

[23] V. P. Carey, Liquid-Vapor Phase-Change Phenomena, New York: Taylor & Francis, 2008.

[24] M.G.Cooper and A.J.P.Lloyd, "The Microlayer in Nucleate Pool Boiling," International Journal of Heat and Mass Transfer, vol. 12, no. 8, pp. 895-913, 1969.

[25] S. T. Hsu and F. W. Schmidt, "Measured Variations in Local Surface Temperatures in Pool Boiling of Water," Journal of Heat Transfer, vol. 83, no. 13, pp. 254-260, 1961.

[26] C. N. Hunter, N. R. Glavin, C. Muratore, T. S. Fisher, J. G. Jones, S. A. Putnam, A. N. Khramov and C. H. Li, "Micro-patterned Substrates with Nano-scale Elements for Pool Boiling," in the ASME/JSME 2011 8th Thermal Engineering Joint Conference, Honolulu, Hawaii, USA, 2011.